HHS Public Access

Author manuscript

Cancer Res. Author manuscript; available in PMC 2021 March 01.

Published in final edited form as:

Cancer Res. 2020 September 01; 80(17): 3692–3705. doi:10.1158/0008-5472.CAN-20-0530.

Deletion of Glutathione S-Transferase Omega 1 Activates Type I Interferon Genes and Downregulates Tissue Factor

Yibin Xu[1,2], **Armand Bankhead III**[2,3], **Xiaoli Tian**[1,2], **Jianming Tang**[1,2], **Mats Ljungman**[2,4,5], **Nouri Neamati**[1,2,*]

[1]Department of Medicinal Chemistry, College of Pharmacy, University of Michigan, Ann Arbor, MI, USA

[2]Rogel Cancer Center, University of Michigan, Ann Arbor, MI, USA

[3]Department of Biostatistics and Department of Computational Medicine and Bioinformatics, Ann Arbor, MI, USA

[4]Department of Radiation Oncology, University of Michigan, Ann Arbor, MI, USA

[5]Department of Environmental Health Sciences, University of Michigan, Ann Arbor, MI, USA

Abstract

Glutathione S-transferase omega 1 (GSTO1) is an atypical GST isoform that is overexpressed in several cancers and has been implicated in drug resistance. Currently, no small-molecule drug targeting GSTO1 is under clinical development. Here we have validated GSTO1 as an impactful target in oncology. Transcriptional profiling coupled with proteomics uncovered novel pharmacodynamic markers and cellular pathways regulated by GSTO1. CRISPR/Cas9 GSTO1 knockout (KO) cell lines failed to form tumors or displayed growth delay *in vivo*; they also formed smaller 3D spheroids *in vitro*. Multi-omics analysis in GSTO1 KO cells found a strong positive correlation with cell adhesion molecules and interferon response pathways and a strong negative correlation with Myc transcriptional signature. Additionally, several clinically used drugs showed significant synthetic lethality with loss or inhibition of GSTO1. Transcription and protein expression of tissue factor (gene name, F3) were downregulated in response to GSTO1 KO. F3 is associated with poor patient survival and promotion of tumor progression in multiple cancers and is a known risk factor for metastasis. Transcription of F3 was regulated by IL-1β, whose secretion decreased upon inhibition of GSTO1, suggesting that IL-1β links GSTO1 expression and F3 transcription. In summary, our results implicate GSTO1 as a potential therapeutic target in cancer and offer new mechanistic insights into its significant role in cancer progression.

Keywords

Glutathione S-transferase Omega 1 (GSTO1); Integrated Omics Studies; Tissue Factors; Type I Interferon; Synthetic Lethality

[*]**Corresponding author**: Dr. Nouri Neamati, Department of Medicinal Chemistry, College of Pharmacy, Rogel Cancer Center, University of Michigan, Ann Arbor, MI, USA, Phnoe number: +1 734 647 2732, neamati@umich.edu.

Conflict of interest: The authors declare no conflict of interest.

Introduction

Glutathione S transferase omega 1 (GSTO1), a member of the cytosolic glutathione S transferase (GSTs) family, is widely expressed in human tissues (1). GSTs are important detoxifying enzymes that catalyze the conjugation of electrophilic substrates to glutathione, and play a critical role in cellular detoxification (2). With a cysteine residue present in the active site instead of a tyrosine commonly found in other glutathione S transferases, GSTO1 carries distinct enzymatic and metabolic functions. It plays important roles in biotransformation of xenobiotics, glutathionylation, deglutathionylation, and redox detoxification (3). GSTO1 overexpression and polymorphism correlate with several pathological diseases including neurological disorders, cancers, and inflammatory diseases (3).

GSTO1 is up-regulated in several human cancers including esophageal squamous cell carcinoma (4,5), colorectal (5,6), and urinary bladder cancer (7). However, how GSTO1 is mechanistically linked with disease progression is largely unknown. GSTO1 overexpression is associated with drug resistance (8,9), and GSTO1 inhibitors have shown to sensitize cancer cell to cisplatin (5,10). GSTO1 expression is also induced by chemotherapy and its knockdown halts breast cancer stem cell enrichment (11). Knockdown of GSTO1 leads to cell apoptosis in colorectal (5) and erythroleukemia cell lines (12) and causes significant reduction in cell survival (13). The glutathionylation of intracellular protein serves as an essential post-translational modification modulating signal transduction (14,15), and exert diverse impact on cellular processes. The glutathionylation/deglutathionylation function positions GSTO1 as a key regulator of critical proteins in cell growth pathways (16,17). Moreover, GSTO1 is crucial in modulating the Toll-like receptor 4 (TLR4)-mediated pro-inflammatory pathway (18), promoting NLRP3 inflammasome activation (19) and attenuating the release of pro-inflammatory cytokines including interleukin-1β (IL-1β), interleukin-6 and tumor necrosis factor (TNF) (20), which are important in the tumor immune environment. GSTO1 may significantly contribute to various pathologies; however, the roles of GSTO1 in cancer progression are largely unexplored.

To fully characterize the roles of GSTO1 in cancer progression, we employed CRISPR/Cas9 to knockout GSTO1 in multiple cancer cell lines and evaluated its impact using a variety of phenotypic and genomic profiling. Our results demonstrate that depletion of GSTO1 suppressed tumor growth *in vivo* and inhibited three-dimension (3D) spheroid growth *in vitro*. Using multi-omics genome-wide profiling (Bru-seq, RNA-seq, and MS proteomics), we have characterized the transcriptional and translational response to GSTO1 deletion. Loss of GSTO1 caused transcriptional suppression of genes involved in cell cycle checkpoints, as well as target genes for Myc and E2F transcription factors. Furthermore, genes and proteins involved in cell adhesion, interferon alpha (IFN α) and interferon gamma (IFN γ) response were enriched in GSTO1 KO cells. On the basis of transcriptome signature of GSTO1 KO cells, we tested select FDA-approved drugs in GSTO1 KO cells and expanded the utility of GSTO1 inhibitors in combination with standard-of-care drugs. Cumulatively, our study demonstrates the significance of GSTO1 in cancer progression, reveals extensive regulation of gene expression by GSTO1, and further validates GSTO1 as a therapeutic target in cancer.

Materials and Methods

Cell lines

HCT116 (ATCC, CCL-247) and GSTO1 KO cells were cultured in RPMI 1640 supplemented with 10% fetal bovine serum. U-87 MG (generously provided by Dr. Alan L. Epstein (University of Southern California, Los Angeles, CA)), A172 (ATCC, CRL-1620) and their related GSTO1 KO cells were cultured in Dulbecco's minimal essential media supplemented with 10% fetal bovine serum. Cells were kept at 37°C in a humidified atmosphere of 5% CO2. All cell lines were maintained in culture under 30 passages and tested regularly for Mycoplasma contamination using PlasmoTest.

Reagents

CB-839, mitomycin C, cryptotanshinone, altretamine, GSK583, liproxstatin-1, spautin-1, PD-1/PD-L1 inhibitor 2, RVX-208, selinexor, ferrostatin-1, diacerein, LY2603618, and patupilone were purchased from Selleckchem (Houston, TX). Cisplatin, carboplatin and oxaliplatin were purchased from Sigma-Aldrich (St. Louis, MO). Olaprib, niraparib, veliparib were purchased from Cayman Chemical (Ann Arbor, MI). As_2O_3 was purchased from BioTang (Lexington, MA). C1–27 is a GSTO1 inhibitor previously identified and synthesized by our laboratory (5).

CRISPR/Cas9 mediated genome editing

GSTO1 knockout cancer cell lines were generated using the Edit-R CRISPR-Cas9 system from Dharmacon (GE Healthcare, Lafayette, CO). Edit-R Lentiviral hEF1α-Blast-Cas9 lentiviral particles (generously provided by Phillip L. Palmbos, University of Michigan, MI) were transduced into U-87 MG, HCT116 and A172 cells and stable Cas9 expressing lines were generated by blasticidin selection. Cells were co-transfected with tracrRNA and GSTO1-targeting crRNA (CM-011950–01-0002) specific for exon 2 or non-targeting crRNA control (U-002000–05). Individual colonies were further selected and screened for loss of GSTO1 expression. Targeted mutations were confirmed using Sanger sequencing.

Animal studies

Female NOD/SCID mice, 6–10 week old, were used for implantation of HCT116 survival experiments. Female ICRSC mice, 6–10 week old, were used for implantation of HCT116 and U-87 MG tumor monitoring experiments. 1×10^6 HCT116 or 2×10^6 U-87 MG tumor cells were implanted subcutaneously into right flank regions of mice. Tumor growth was monitored twice a week by digital caliper and tumor volumes were calculated by the (length × $width^2$)/2 equation. Mice were sacrificed once tumors reached 1500 mm^3. The University of Michigan Institutional Animal Care and Use Committee approved all animal experiments.

Pan-disease gene expression analysis

Patient data described in this work were in part based upon data generated by the TCGA Research Network: http://cancergenome.nih.gov/. Patient sample RNA-seq RSEM normalized gene expression values and related survival metadata were sourced from the TCGA GDAC Firehose (21). When multiple samples were available for a given patient,

barcodes were sorted alphabetically and the first was selected for analysis. 9,718 total samples were evaluated across 34 total disease groups.

TCGA gene expression data downloaded from GDAC Firehose is upper-quartile normalized for comparison within disease groups. To survey GSTO1 expression across all 34 TCGA disease groups we normalized log2 RSEM expression values by calculating z-scores for each patient using the following steps for each patient: 1) Calculate the patient mean and patient standard deviation for all protein-coding gene expression values 2) Calculate GSTO1 z-score by subtracting the patient mean and dividing by the patient standard deviation. The resulting GSTO1 z-scores are shown in Figure 1A.

TCGA disease patient samples were evaluated for reduced survivability by comparing survival outcomes for patients with high and low expression of GSTO1. Thresholding for high and low expression patient populations was evaluated using five different quantile cutoffs: 95%, 90%, 75%, 50%, and 25%. A log-rank test statistic was calculated for each cutoff to compare the survival distributions of high and low expression patient populations with the null hypothesis that there was no difference in survival curves. *p*-values were FDR adjusted across all diseases and quantile cutoffs. To reduce over-fitting of a single expression cutoff per disease, associations with reduced survival were required to have FDR adjusted *p*-values ≤ 0.1 for at least two quantile cutoffs. Survival analysis statistics were calculated using the R statistical programming language (22).

Gene set enrichment analysis (GSEA) was used to identify the enrichment of pathways with genes that are co-expressed with GSTO1. GSEAv2.2.3 was used with v6 gene sets sourced from MSigDB. 10,000 gene set permutations were performed using weighted mode scoring and Pearson metric (23). Only genes with evidence of expression in >50% of a disease patient population were considered. Five diseases were evaluated based on association with reduced survivability (SKCM, GBMLGG, KIRC, STAD, UVM).

Bru-seq analysis of nascent RNA synthesis

Bru-seq analysis was performed as previously described (24). Briefly, when cells reached 80–90% confluence, bromouridine (final concentration of 2 mM) was added to the media to label newly synthesized nascent RNA for 30 min. Cells were collected in TRIzol (Invitrogen, Waltham, MA) and total RNA was isolated. Bru-labeled, nascent RNA was isolated, converted into cDNA libraries and sequenced using an Illumina HiSeq 2000 sequencer (University of Michigan DNA Sequencing Core, MI). Sequencing reads were mapped to the hg38 reference sequence. Ensemble gene identifiers were mapped to HGNC symbols and Entrez identifiers using Gencode v27 annotations (25). Only measurements mapping to protein coding genes with entrez identifiers were considered and gene changes with absolute fold change > 2 and mean RPKM > 0.5 were considered significant.

RNA-seq profiling

Cells were lysed with TRIzol® Reagent (ThermoFisher Scientific, Waltham, MA) at room temperature. RNA was further purified with DirectZol kit (Zymo Research, Irvine, CA). RNA quality was assessed using the TapeStation (Agilent Technologies, Santa Clara, CA). Samples with RINs (RNA Integrity Numbers) of 8 or greater were prepared with TruSeq

Stranded mRNA Library Prep (Illumina) per the supplier's protocol with 1μg of RNA and 12 cycles of PCR amplification. Libraries were checked for size on the TapeStation and quantified using the Kapa Biosystems library quantification kit (Illumina). The libraries were barcoded, pooled and sequenced using 50b paired-end 50bp (U-87 MG, University of Michigan DNA Sequencing Core, Ann Arbor, MI) and single-end 50bp (HCT116, University of Michigan DNA Sequencing Core, MI) sequencing. Reads were mapped to GRCh38 using STAR v2.5.2 (26) and gene quantifications were calculated using Cufflinks v2.2.1(27) to quantify refGene annotations. Gene read counts calculated using featureCounts (28) v1.6.1 were used to evaluate differential expression using DESeq2 v1.18.1(29). Protein coding genes were considered significantly differentially expressed with a mean FPKM > 0.5 and absolute fold change > 1.5 and FDR adjusted p-value < 0.05. All gene readouts where required to be mappable to both an HGNC and Entrez identifier to be considered for gene set enrichment analyses. This data has been deposited in NCBI's Gene Expression Omnibus and are accessible through GEO Series accession number GSE147626 (https://www.ncbi.nlm.nih.gov/geo/query/acc.cgi?acc=GSE147626) (30).

TMT labeling and liquid chromatography-mass spectrometry analysis

HCT116 nt WT and GSTO1 KO cells (triplicate each) were lysed with RIPA buffer (ThermoFisher Scientific, 89901), followed by sonication and centrifugation at 10000 × g for 15 min at 4 °C. The supernatant was saved and protein concentration determined by the BCA assay (ThermoFisher Scientific, 23225). 75 μg of protein was used to perform tandem Mass Tag (TMT) labeling with the TMT 6-plex™ isobaric labeling kit (ThermoFisher Scientific, Waltham, MA) essentially according to the manufacturer's protocol. Briefly, upon reduction and alkylation of cysteines, the proteins were precipitated by adding 6 volumes of ice-cold acetone followed by overnight incubation at −20° C. The precipitate was spun down, and the pellet was allowed to air dry. The pellet was resuspended in 0.1M TEAB and overnight digestion with trypsin (1:50; enzyme:protein) at 37 ° C was performed with constant mixing using a thermomixer. The TMT 6-plex reagents were dissolved in 41 μl of anhydrous acetonitrile and labeling was performed by transferring the entire digest to TMT reagent vial and incubating at room temperature for 1 h. Reaction was quenched by adding 8 μl of 5% hydroxyl amine and further 15 min incubation. Labeled samples were mixed together, and dried using a vacufuge. An offline fractionation of the combined sample (~200 μg) into 8 fractions was performed using high pH reversed-phase peptide fractionation kit according to the manufacturer's protocol (Pierce, 84868). Fractions were dried and reconstituted in 9 μl of 0.1% formic acid/2% acetonitrile in preparation for LC-MS/MS analysis.

In order to obtain superior quantitation accuracy, we employed multinotch-MS3 (McAlister GC) which minimizes the reporter ion ratio distortion resulting from fragmentation of co-isolated peptides during MS analysis. Orbitrap Fusion (Thermo Fisher Scientific, Waltham, MA) and RSLC Ultimate 3000 nano-UPLC (Dionex, Sunnyvale,CA) was used to acquire the data. 2 μl of the sample was resolved on a PepMap RSLC C18 column (75 μm i.d. × 50 cm; Thermo Scientific) at the flow-rate of 300 nl/min using 0.1% formic acid/acetonitrile gradient system (2–22% acetonitrile in 150 min;22–32% acetonitrile in 40 min; 20 min wash at 90% followed by 50 min re-equilibration) and directly spray onto the mass spectrometer

using EasySpray source (Thermo Fisher Scientific, Waltham, MA). Mass spectrometer was set to collect one MS1 scan (Orbitrap; 120K resolution; AGC target 2×105; max IT 100 ms) followed by data-dependent, "Top Speed" (3 seconds) MS2 scans (collision induced dissociation; ion trap; NCE 35; AGC 5×10^3; max IT 100 ms). For multinotch-MS3, top 10 precursors from each MS2 were fragmented by HCD followed by Orbitrap analysis (NCE 55; 60K resolution; AGC 5×104; max IT 120 ms, 100–500 m/z scan range).

Proteome Discoverer (v2.4, Thermo Fisher, Waltham, MA) was used for data analysis. MS2 spectra were searched against SwissProt human protein database using the following search parameters: MS1 and MS2 tolerance were set to 10 ppm and 0.6 Da, respectively; carbamidomethylation of cysteines (57.02146 Da) and TMT labeling of lysine and N-termini of peptides (229.16293 Da) were considered static modifications; oxidation of methionine (15.9949 Da) and deamidation of asparagine and glutamine (0.98401 Da) were considered variable. Identified proteins and peptides were filtered to retain only those with FDR≤1%. Quantitation was performed using high-quality MS3 spectra (Average signal-to-noise ratio of 10 and <30% isolation interference). Protein changes with absolute fold change > 1.5 and qval < 0.1 were considered significant.

Bru-seq and RNA-seq gene set enrichment

Gene set enrichment was performed using DAVID and GSEA. The RDAVIDWeb services Bioconductor package was used to identify KEGG and GO Biological Process categories that were enriched for differentially expressed genes regardless of fold change direction (31). GSEAv2.2.3 was used with v6.1 gene sets sourced from MSigDB to identify gene sets significantly up or down regulated. 10,000 gene set permutations were performed using weighted mode scoring of genes ranked using DESeq2 shrunken log fold change APEGLM method (32). Gene sets with FDR adjusted *p*-values < 0.05 were considered significant.

3D spheroid culture

Indicated number of cells were plated in non-adherent U bottom 96 well plate (Corning, 4520) with 5% collagen (Stem Cell Technologies, Cambridge, MA) in original medium (100 μl). Additional 100 μl of medium with 5% collagen was gently added on day 4. Images of spheroids were taken using 10X objective on an Olympus IX83 motorized inverted microscope with cellSens™ Dimension software (Olympus Corporation, Waltham, MA). For viability assay, 100 μl CellTitre-Glo 3D (Promega, G9681) were added to each well. Luminescence was measured on Synergy H1Hybrid Multi-Mode Reader (BioTek, Winooski, VT).

Sphere-formation assay

Cells were dissociated and seeded in ultra-low attached plates (Corning, 3474 or 3473) and cultured in serum-free medium (X-VIVO™ 20, Lonza, 04–448Q) for 10 days. Floating spheres in three fields per each sample were counted and images of spheroids were taken using 10X objective on an Olympus IX83 motorized inverted microscope with cellSens™ Dimension software (Olympus Corporation, Waltham, MA).

Western blot

Western blotting was performed to test GSTO1 expression of knockout cells and other related biomarkers. Cells were lysed in RIPA buffer (Sigma-Aldrich, R0278) containing protease and phosphatase inhibitors (Thermo Scientific, 78442). 30 μg extracts from each sample was electrophoresed on Bis-Tris gel and transferred to a polyvinylidene difluoride membrane (Bio-Rad, 1704274). Primary antibodies (Anti-GSTO1 antibody, Gene Tex, GTX105655, 1:2000; Anti-TF antibody, Santa Cruz Biotechnology, sc-393657, 1:500; Anti-GAPDH antibody, Cell Signaling, 2118S, 1:1000) were applied overnight at 4C in 5% BSA (Calbiochem, 2930) followed by secondary antibody. The membranes were imaged by the Odyssey Imaging Systems (LICOR, Lincoln, NE).

Results

GSTO1 is up-regulated in select cancers and correlates with decreased patient survival

An initial pan-cancer patient survey of GSTO1 expression analysis was performed using RNA-seq, survival, and disease progression read-outs from 9,718 patients across 34 tumor types. RNA-seq data from each patient was z-score normalized and we found that GSTO1 expression was well above average (z-score = 0) across all 34 tumor types (Fig. 1A). We identified five tumor types for which high GSTO1 expression was associated with reduced survival (Fig. 1B): glioblastoma and lower grade glioma (GBMLGG), kidney renal clear cell carcinoma (KIRC), skin cutaneous melanoma (SKCM), stomach adenocarcinoma (STAD) and uveal melanoma (UVM). This association of GSTO1 expression and poor survival was also observed across other non-TCGA glioma cohorts (Supplementary Fig. S1A). In addition, we observed a clear increase in GSTO1 expression with cancer disease progression. Glioma patients with more aggressive disease (GBM) expressed significantly more GSTO1 than patients with low grade glioma (LGG) (Supplementary Fig. S1B). GSTO1 expression also increased with KIRC tumor stage and grade (Supplementary Fig. S1C). These results show that increased expression of GSTO1 is associated with poor patient survival and disease progression in multiple cancers, suggesting that GSTO1 plays an important role in tumor progression.

GSTO1 depletion suppresses *in vivo* tumor growth

To investigate the function of GSTO1 in cancer, we used CRISPR/Cas9 to knock out GSTO1 in three representative cell lines (A172, HCT116, U87-MG) with high expression of GSTO1 (Fig. 2A). Deletion of GSTO1 was verified at both the protein (Fig. 2B, Supplementary Fig. S2A) and mRNA level (Supplementary Fig. S2B). Sanger sequencing further validated that the genome editing was caused by deletions and frameshifts in exon 2 of the *GSTO1* gene (Supplementary Fig. S2C, one clone for each cell line).

To directly explore the role of GSTO1 in tumorigenesis, we tested the tumor growth of GSTO1 KO cells and their non-targeted wild-type counterparts (nt WT) in xenograft models in ICRSC or NOD/SCID mice (n=5). Strikingly, GSTO1 KO HCT116 cells showed remarkably reduced tumor burden as compared to nt WT cells (Fig. 2C, 2F). Furthermore, in an independent experiment, the HCT116 GSTO1 KO group had significantly prolonged survival (log-rank p=0.032) for up to four weeks as compared to the nt WT group (Fig. 2E).

Loss of GSTO1 in U-87 MG cells inhibited tumor formation (Fig. 2D, 2F), and no tumors were detected even after reinjection of U-87 MG GSTO1 KO cells and extension of tumor monitoring for an additional four weeks. Despite numerous attempts to implant A172 cells *in vivo*, multiple strategies failed to generate tumor in flanks of mice.

In conclusion, these results demonstrate that the loss of GSTO1 significantly suppresses tumor growth *in vivo* for both HCT116 and U-87 cells suggesting that GSTO1 is an impactful therapeutic target in cancer.

Deletion of GSTO1 hampers U-87 MG cell proliferation

To understand underlying mechanism of the growth inhibition *in vivo*, we first determined whether CRISPR/Cas9-mediated loss of GSTO1 affected cell proliferation. We measured the doubling time of nt WT and three single clones in all three GSTO1 KO cell lines (Fig. 3A) to avoid characterization of single clone behaviors. Interestingly, depletion of GSTO1 in U-87 MG cells slowed cell growth, but had no significant effect on the growth of HCT116 and A172 cells. Consistent with this finding, loss of GSTO1 in U-87 MG cells significantly decreased the numbers and sizes of cell colonies, but had little effect on HCT116 and A172 cells (Fig. 3B). It should be noted that the three HCT116 GSTO1 KO clones grew at different rates, possibly due to variations in single clone behavior.

In summary, our results demonstrate that deletion of GSTO1 significantly reduced U-87 MG *in vitro* cell proliferation, indicating that GSTO1 is essential for *in vitro* cell growth in certain cell types. Interestingly, GSTO1 KO affected HCT116 tumor growth *in vivo* but not *in vitro* 2D culture.

GSTO1 KO impedes the growth of 3D tumor spheroids

Due to the difference in access to nutrients, oxygen and multi cellular 3D contacts, cells grown in 3D culture are of phenotypic heterogeneity and in that sense resemble *in vivo* tumors. In particular, 3D culturing incorporates some aspects of the tumor microenvironment, including cell adhesion and crosstalk with extracellular matrix (ECM) (33).

As described above, HCT116 GSTO1 KO cells showed significant tumor growth delay while no difference in growth rate was observed when grown in 2D culture, suggesting that deletion of GSTO1 may affect the tumor microenvironment. To test this hypothesis, we generated 3D tumor spheroid models for each cell line (Fig. 3C and Supplementary Fig. S3A–B for other single clones). Interestingly, we found that HCT116 KO cells showed significant retardation of cell proliferation in 3D culture despite no observed difference in growth rate in 2D culture. The growth rate is measured by the diameter of spheroids and was further assessed by CellTiter-Glo® 3D cell viability assay, which measures the presence of metabolically active cells (Fig. 3D–E). We also observed that spheroids of HCT116 nt WT cells were more invasive than those of KO cells. U-87 MG GSTO1 KO 3D tumor spheroids grew slower than those of the nt WT, which was also reflected in 2D culture. A172 cells formed a monolayer and failed to form proper spheroid structures over collagen (Fig. 3D–E). Although GSTO1 did not affect HCT116 cell growth in 2D culture, it significantly

inhibited 3D cell growth, further supporting the hypothesis that GSTO1 influences vital pathways involved in cell adhesion and ECM crosstalk.

Depletion of GSTO1 inhibits neurosphere formation in U-87 MG

In agreement with the observed slow growth rate of U-87 MG GSTO1 KO cells in mono-layer and 3D cultures, the growth of these cells as xenografts *in vivo* was also blocked. One hypothesis for this behavior is that GSTO1 affects cancer stem cell survival. Studies have shown that HIF-dependent induction of GSTO1 expression promotes chemotherapy-induced breast cancer stem cell enrichment (11). Therefore, we next sought to test if GSTO1 depletion affects the survival of cancer stem cells. Growing cells as neurospheres enriches for cancer stem cells (CSCs) or cells with progenitor characteristics (34). Interestingly, deletion of GSTO1 in U-87 MG cells inhibited neurosphere formation (Fig. 3F–G). This phenotype was consistent for all U-87 MG GSTO1 clones tested (Supplementary Fig. S4). We further assessed the neurosphere formation in A172 cells and found that deletion of GSTO1 didn't impact the size or number of neurospheres. HCT116 GSTO1 KO cells display small tumor spheroids as compared to the nt WT (p-value < 0.05, Fig. 3F–G). In conclusion, GSTO1 expression is required for spheroid formation in two of the three cell lines examined.

Integrated transcriptional profiles across cell lines reveals GSTO1 dysregulates critical pathways in cancer

To obtain a comprehensive molecular understanding of GSTO1 function in cancer, we performed in-depth nascent RNA Bru-seq on non-targeted wild-type parental cells and GSTO1 KO U-87 MG (clone 1, n=1), HCT116 (clone 1, n=1), and A172 (clone 1, n=1) cells (24). Depletion of GSTO1 caused a strong perturbation of transcription in U-87 MG with less effect observed in HCT116 and A172 cells (Fig. 4A, top 30 up- or down-regulated genes in Supplementary Tables S1–6). A number of genes were similarly transcriptionally affected by GSTO1 loss in the HCT116 and U-87 MG cell lines (up-regulated: p=9.37e-15, down-regulated: p=0.00205) (Fig. 4B, commonly up- or down-regulated gene sets in Supplementary Table S7). However, there was little overlap between the changes in these two cell lines and the A172 cell line (Supplementary Fig. S5A). Thus, we focused our subsequent analyses on HCT116 and U-87 MG cells. We used gene set enrichment analysis (GSEA) to identify gene sets significantly enriched for genes changing in response to loss of GSTO1 (Supplementary Fig. 5B and Supplementary Tables S8–13). DNA repair, p53 pathway and negative regulation of protein binding gene sets were significantly up-regulated in both HCT116 and U-87 MG cells after loss of GSTO1 (Fig. 4C and Supplementary Fig.S6A). In U-87 MG cells, loss of GSTO1 resulted in the up-regulation of UV response gene sets (Supplementary Fig. S6B) along with DNA repair gene sets. In addition, genes involved in epithelial mesenchymal transition were down-regulated in response to loss of GSTO1 in U-87 MG cells (Supplementary Fig. S6C). In HCT116 cells, deletion of GSTO1 caused significant up-regulation of gene sets related to interferon production, interferon responses, and interferon related signaling pathways (Supplementary Fig. S6D). Gene sets related to tight junction and apical junction were also up-regulated, while Myc-target gene sets were down-regulated in response to GSTO1 KO in HCT116 (Supplementary Fig. S6E).

We also performed RNA-seq on U-87 MG (n=3, clone 1) and HCT116 (n=3, clone 1) GSTO1 KO cells (Fig. 4D, top 30 dysregulated genes in Supplementary Tables S14–17). Similar to the nascent RNA transcription profile, U-87 MG had a larger number of differentially expressed genes as compared to HCT116. The two cell lines shared 77 down-regulated genes and 191 up-regulated genes (Fig. 4E) (p = 1.06e-59 and p =3.42e-14, respectively). Significantly down-regulated gene sets shared by HCT116 and U-87 MG included E2F targets, MYC targets and G_2M checkpoint (Fig. 4F and Supplementary Tables S18–19). Although G_2M checkpoint genes were up-regulated in both cell lines, a difference in growth rate was only observed in U-87 MG cells. One potential explanation is that additional compensatory pathways were inhibited or activated to maintain cell growth regardless of G_2M checkpoint activation in HCT116 cells. Interestingly, compared to 11 up-regulated gene sets in U-87 MG, we observed 182 uniquely up-regulated gene sets in HCT116 including Notch and VEGF signaling pathway, which may provide insight to these compensatory effects. Similar to Bru-seq findings for the HCT116 cells, the up-regulated gene sets following GSTO1 loss included complement and coagulation cascades, detection of biotic stimulus and positive regulation of interferon alpha (IFN-α) production (Fig. 4F and Supplementary Table S20–21), suggesting that GSTO1 deletion augments the transcription of innate immune system related pathways.

We further analyzed gene sets co-expressed with GSTO1 in patient samples (Fig. 4G and Supplementary Table S22–26). Thirty-seven gene sets were commonly enriched in GBMLGG, KIRC, SKCM, STAD and UVM, including Parkinson's diseases, Huntington disease, Alzheimer's disease, antigen processing and presentation and reactive oxygen species. As mentioned in the introduction, GSTO1 has been shown to be involved in the reactive oxygen species pathway; this finding, while not novel, shows that GSTO1 co-expression in TCGA patient cohorts is able to re-capitulate known canonical biological function of GSTO1. Additionally, several reports indicate that GSTO1 plays important roles in neurodegenerative diseases (35,36) and inflammation (17,19). This validates our co-expression analysis, and highlights the novelty of our findings. Similar to our Bru-seq and RNA-seq results, gene sets involved in DNA repair, UV response and Myc-targets gene sets were also enriched in multiple disease types. Interferon alpha response gene set was enriched in four disease types including GBMLGG, SKCM, STAD and UVM. These findings using GSTO1 co-expression in patient gene expression across multiple disease cohorts further support the clinical relevance of our *in vivo* and *in vitro* GSTO1 KO results and further shed light on the molecular pathways modulated by GSTO1.

Annotation of transcriptional profiles reveals the role of GSTO1 in tumor microenvironment, epithelial-mesenchymal transition, proliferation and cancer immune responses

A feedback effect at the transcriptional or translational level is common when cells lose the function of a gene. Numerous studies have highlighted that compensatory mechanisms induced by genetic mutation events contributed largely to the phenotypes (37). To further study the transcriptional changes induced upon GSTO1 loss, we used DAVID to perform an over-representation gene set enrichment analysis by combining the significantly up-regulated and down-regulated genes (FC>1.5, FDR q-value<0.1) (Fig. 4H and

Supplementary Tables S27–28). HCT116 and U-87 MG cell lines shared twenty-four enriched gene sets (Supplementary Fig. S7). Deletion of GSTO1 had a significant impact on gene sets related to angiogenesis (GO:0001525, GO:114814 and GO:1901342), cell adhesion (GO:0022409) and ECM interaction (GO:0007160 and hsa04512), further supporting the role of GSTO1 in modulating the tumor microenvironment. Several gene sets involved in cell migration are significantly enriched (GO:0010631, GO:0043542, GO:0090132 and GO:0051272). Gene sets involved in cell proliferation (GO:0050678 and GO:0050673), differentiation (GO:0042692) and apoptosis (GO:2001236) are also enriched for genes changing in response to GSTO1 KO. Interestingly, we also found 13 gene sets related to immune response which is consistent with previous studies showing GSTO1's relationship with inflammation and immune response (17,19,20). Deletion of GSTO1 in tumor cells significantly enriched the transcription of gene sets in cytokine production, signaling pathways, and cellular responses, including type I interferon (GO:0035455, GO:0034340 and GO:0060337) and tumor necrosis factor (GO:0032640, GO:0032680 and GO:1903555). T cell activation gene sets (GO:0042110) were also enriched in both GSTO1 cell lines, suggesting that GSTO1 may be involved in the activation of T cells.

These results highlight the multi-faceted nature of GSTO1 function in tumor progression through modulation of tumor microenvironment, cell proliferation and differentiation, epithelial-mesenchymal transition and immune response.

In-depth multi-omics analysis in HCT116 cells reinforces impact of GSTO1 in cell adhesion and interferon responses

Nascent mRNA expression, mRNA expression and steady-state protein levels may not always correlate due to post-transcriptional, translational and protein degradation regulation (38). Thus, a joint analysis of the transcriptomic and proteomic profiles provides more detailed insights that may not be deciphered from individual analysis. In addition to transcriptome profiling, we performed mass spectrometry-based proteomic profiling to provide further insight into the regulatory programs impacted by GSTO1 KO in HCT116 cells (Fig. 5A, top 30 significantly changed proteins in Supplementary Tables S29–30). Differential expression was used to quantify significant changes across all 3 platforms (Materials and Methods) and used to identify four genes and proteins that were commonly down-regulated and twelve genes and proteins that were commonly up-regulated in the data sets generated from Bru-seq, RNA-seq and mass spectrometry proteomic profiling (Fig. 5B). SLC2A1, which was down-regulated across all three platforms, encodes for glucose transporter type 1 (GLUT1), an important glucose transporter in the glycolytic pathway. GLUT1 has been associated with tumor progression and poor prognosis in many human solid tumors (39). GLUT1 gene transcription is promoted by c-Myc (40) while suppressed by wild-type p53(41). Our observation that GSTO1 deletion down-regulates MYC target genes and the DNA repair pathway is consistent with such regulation. We found that the interferon-stimulated gene IFIT1 was transcriptionally up-regulated following loss of GSTO1. Interestingly, IFIT1 expression is commonly down-regulated in cancer patients (42) and its higher expression correlated with improved clinical outcome (43). Thus, targeting of GSTO1 may improve clinical outcome by causing up-regulation of IFIT1.

We further conducted gene set enrichment analysis (GSEA) to identify GSTO1 direction-specific regulatory effects across all three platforms (Supplementary Tables S31–32). Consistent with the DAVID enrichment results, cell adhesion molecules, interferon alpha response, and interferon gamma response gene sets were up-regulated (Fig. 5C–D). Myc target gene sets were down-regulated in RNA-seq and Bru-seq datasets, but not at the protein level. Limited by detection sensitivity of mass spectrometry, proteomics results covered a smaller proportion of corresponding genes, which complicated a direct comparison between the different platforms. Despite differences in coverage, high consistency among the three platforms were observed in cell adhesion molecules gene set covering 107 differentially expressed genes (Fig. 5E). Strikingly, the up-regulation of interferon alpha response was concordant not only among the three platforms in HCT116 cells, but also in U-87 MG (RNA-seq/Bru-seq) and in A172 (Bru-seq) (Fig. 5F). This strong agreement between platforms and cell lines reinforces the relevance of GSTO1 to cell adhesion and interferon response as potential mechanism by which GSTO1 contributes to tumor progression.

Tissue factor expression is regulated by GSTO1 and shows significant correlation in patient samples

Nascent RNA (Bru-seq), steady-state RNA (RNA-seq) and protein profiling (MS) of control and GSTO1 KO HCT116 and U-87 MG cells revealed that Tissue factor gene (*F3*) was significantly down-regulated as compared to the corresponding Cas9 non-targeted control cells across all platforms in both cell lines (Fig. 5B, Fig. 6A). Consistent with *F3* down-regulation in GSTO1 KO cell lines, nascent transcription of *F3* was also down-regulated in siGSTO1-treated and GSTO1 inhibitor **C1–27**-treated HCT116 (Fig. 6B). We further confirmed the down-regulation of tissue factor protein (TF) following the loss of GSTO1 in cells and tumor samples using Western blot (Fig. 6C). These results suggest that TF transcription is regulated by GSTO1.

TF is a crucial mediator of tumor cell proliferation, metastasis and the tumor microenvironment (44). High expression of *F3* in patient samples significantly correlates with patient survival, suggesting that *F3* is essential for tumor progression. We further explored the correlation of GSTO1 and *F3* expression in patients. Strikingly, in colorectal cancer (n=64), expression of GSTO1 was significantly correlated to *F3* expression (Fig. 6D), further validating the molecular link between GSTO1 and *F3*. Interestingly, we observed that in glioblastoma stem cells (n=20), *F3* RNA expression also showed remarkable correlation with GSTO1 expression (Fig. 6E). Additionally, tissue factor promotes cancer stem cell activity and serves as a therapeutic oncotarget for the eradication of cancer stem cells (45).

Taken together, we identified that TF was suppressed upon GSTO1 knockdown and its expression correlated with GSTO1 expression in multiple cancer data sets. These results suggest that GSTO1 is important in regulating *F3* transcription, further supporting an important role of GSTO1 in tumor progression.

Platinum drugs, PARP inhibitors and glutaminase inhibitor CB-839 show synthetic lethality with the loss of GSTO1

An attractive strategy to overcome drug resistance is to target enzymes that exhibit synthetic lethality. To maximize the efficacy of GSTO1 inhibitors, we aimed to identify compounds that exhibit selective cytotoxicity to GSTO1 KO cells, potentially targeting the compensatory pathways caused by the loss of functional GSTO1. We used HCT116 GSTO1 KO cells as our screening platform and further tested synergy using GSTO1 inhibitor **C1–27** (Fig. 7A). Elevated GSTO1 in cancer cells correlates to drug resistance (8,46), and GSTO1 inhibitors sensitizes cells toward cisplatin and other platinum drugs (5,10). We first tested the hypothesis that platinum drugs would be synthetically lethal with the loss of GSTO1 by treating GSTO1 nt WT and KO cell lines with cisplatin, carboplatin and oxaliplatin (Fig. 7B and Supplementary Fig. S8). Results showed that these platiunum drugs all showed stronger cytotoxicity in HCT116 GSTO1 KO cells as compared to the nt WT, suggesting that the platinum drugs synergized with the loss of GSTO1. Nascent transcriptome signatures in response to GSTO1 KO show up-regulation of DNA repair, p53 pathway and G_2M checkpoint gene sets. Based on this, we tested 38 clinical or preclinical drugs including DNA damage inducers, PARP inhibitors, p53 inhibitors, and CDK inhibitors. Out of the thirty-eight agents, thirteen were significantly more potent in cells depleted of GSTO1, including glutaminase inhibitor **CB-839**, mitomycin C, and PARP inhibitors (Fig. 7B and Supplementary Fig. S9). We next combined these drugs with **C1–27**, and found that mitomycin C, **CB-839**, and olaparib all showed synthetic lethality with **C1–27** (Fig. 7C). Our results demonstrate that GSTO1 inhibitors may be used in combination with standard-of-care drugs to synergistically kill cancer cells and highlight the strong potential of GSTO1 inhibitors as a therapeutic treatment for cancer.

Discussion

Although GSTO1 is overexpressed in various cancers, its function in cancer is not fully understood and its relationship to cancer signaling pathways is largely unexplored. In this study, we extensively characterized the function of GSTO1 in diverse genetic backgrounds. Our data demonstrate that deletion of GSTO1 significantly inhibits tumor growth *in vitro* and *in vivo*. Multi-omics (Bru-seq, RNA-seq, and MS proteomics) analysis showed that loss of GSTO1, promoted the down-regulation of gene sets pertaining to tumor progression, microenvironment, metastasis, and immune response. Thus, the therapeutic targeting of GSTO1 can block tumor growth.

Targeting the tumor microenvironment is an important strategy to overcome acquired resistance and metastasis. It is widely accepted that in 3D cultures, adhesive interactions with the surrounding ECM and neighboring cells define cell shape and organization, and influence fundamental cellular behaviors. Phenotypically, GSTO1 KO cells showed significant growth delay in 3D spheroid and tumor growth *in vivo* as compared with the 2D mono-layer culture, suggesting that deletion of GSTO1 causes a tumor-suppressing microenvironment. Consistent with that, pathways essential for tumor microenvironment, such as angiogenesis and ECM-receptor interactions, were also dysregulated in response to GSTO1 KO. A recent study also showed that GSTO1 inhibition resulted in decreased

migration and invasion in sorted breast cancer stem cells (47). In conclusion, our results demonstrate that GSTO1 inhibit 3D cell growth, influence gene sets involved in angiogenesis, cell adhesion and interaction with the surrounding ECM, and play an important role in modifying tumor microenvironment.

As a pro-inflammatory protein, GSTO1 governs the release of pro-inflammatory cytokines such as IL6, IL-1β and TNFα (20). GSTO1 is also a signature gene in both human and mouse IL-4-treated macrophages (48). By deglutathionylating NIMA related kinase 7 (NEK7), GSTO1 promotes activation of NLRP3, which is important for IL-1β and IL-18 maturation (19). There is a broad crosstalk between GSTO1 and diverse cytokines; however, the function of GSTO1 in tumor immune responses is still unclear. In this work, we report for the first time that interferon alpha and gamma responses are induced in response to GSTO1 KO. Interferons (IFNs) have important roles in protecting the host against cancer through effects in tumor cell intrinsic property and in immunoregulatory functions. IFNs have an intrinsic impact on tumor cells by inhibiting proliferation, and modulating apoptosis, differentiation, migration and cell surface antigen expression (49). In addition, IFNs affect different biological processes involved in tumor progression, such as angiogenesis and immunity (49,50). Importantly, IFNs play major roles in activating anticancer immunity and inhibiting the activity of immune-suppressive cells and the conversion of tumor-associated macrophages (49). Through the perturbation of IFN responses, GSTO1 might serve as a promising therapeutic target to influence biological pathways in cancer, affect the tumor environment, and alter tumor-infiltrating immune cell properties. Results from our study suggest that deletion of GSTO1 promotes downstream responses of interferon in tumors, which may affect tumor progression and elicit an immune response, but the mechanisms behind this need to be further explored.

The transcription of G_2M checkpoint gene sets, MYC targets gene sets and E2F targets gene sets were down-regulated following GSTO1 depletion in all three GSTO1 KO cell lines. Up-regulation of MYC and E2F transcriptional targets are known for promoting cell growth and proliferation (51,52). In addition, gene set enrichment analysis using DAVID demonstrated that GSTO1 KO caused transcriptional changes of genes regulating cell proliferation, differentiation, and apoptotic-signaling pathways. Consistent with our findings, studies have shown that several critical proteins involved in cell proliferation and metastasis are deglutathionylated by GSTO1, which might influence their biological function (16,17,53). Collectively, our findings demonstrate that GSTO1 deletion inhibits tumor growth, down-regulates gene sets involved in the cell cycle and impacts MYC and E2F pathways in cancer.

We also reported that *F3* transcription is down-regulated in response to GSTO1 loss or inhibition. Associated with poor patient survival and promotion of tumor progression in multiple types of cancers, TF is also a known risk factor of metastasis (44). Previous studies have revealed that TF is associated with sustaining proliferation signaling, preventing cell death, maintaining cancer stem cell behavior and promoting EMT (54). Decreased TF expression upon GSTO1 deletion may reduce invasion, impair formation of neuro-spheroids, and more importantly, prevent tumor-promoting processes in the tumor microenvironment *in vivo*. *F3* transcription is modulated by several transcription factors. Early growth response gene-1 (EGR-1) regulates TF expression under hypoxic conditions in glioblastoma (55). In

the human endometrium, TF expression could be regulated through Sp1 and Sp3 binding on its promoter (56). TF expression is also activated by the Stat3 transcription factor (57). Importantly, *F3* is under the regulation of Interleukin-l β (IL-1β) (58), and we demonstrate that secretion of IL-1β is decreased upon GSTO1 inhibition (59), suggesting that IL-1β is a potential regulating link between GSTO1 and *F3* transcription. Besides that, Interleukin-lα (IL-lα) and tumor necrosis factor-α (TNF-α) also induce tissue factor in endothelium (60). Previous studies indicated that GSTO1 KO mice produced significantly lower levels of TNF-α, suggesting that TNF- α may also play a role in regulating *F3* transcription. In addition, *F3* expression is upregulated downstream of mutant K-Ras oncogene signaling and inactivation of p53 (61). We also observed that p53 pathway is significantly up-regulated in both HCT116 and U-87 MG cells after loss of GSTO1, which might serve as another mechanism in suppressing *F3* transcription. In conclusion, GSTO1 might affect the transcription of *F3* through multiple mechanisms.

In colorectal biopsies, the increased γH2AX expression is correlated to GSTO1 nuclear translocation during disease progression, suggesting that GSTO1 plays a role in genome instability (6). Here, we report for the first time that GSTO1 deletion up-regulates DNA repair gene sets along with UV response gene sets. Importantly, PARP inhibitors are more toxic in GSTO1 KO cells than in GSTO1 expressing cells and show significant synergy with the GSTO1 inhibitor **C1–27**. Due to the accumulation of unrepaired single strand breaks, PARP inhibition leads to stalling of replication forks, resulting in genomic instability and cell death (62). Similarly, we found that DNA alkylating agent mitomycin-C, showed stronger potency in GSTO1 KO cells. Although temozolomide did not show differential activity in U-87 MG and A172 GSTO1 nt WT and KO cell line (Supplementary Fig. S10), U-87 MG cells were more sensitive towards radiation after GSTO1 deletion (Supplementary Fig. S11). These results suggest that despite the up-regulation of DNA repair genes in response to GSTO1 deletion, GSTO1 KO cells are more vulnerable to DNA damage. It is well accepted that chemotherapeutics such as cisplatin and mitomycin-C increase ROS levels, which contributes to their genotoxicity (63). Increased oxidative stress is also reported to augment the antitumor effect of PARP inhibition (64). Interestingly, GSTO1 knockdown and inhibition increases accumulation of cellular ROS (13), and GSTO1 protects Drosophila to ROS damage (65). The effect of GSTO1 on ROS might be the reason for the transcriptional up-reguation of DNA repair or UV response gene sets and sensitization of GSTO1 KO cells toward DNA damaging agents. Although further studies are needed to elucidate the specific mechanism of mediating DNA damage and repair, our study for the first time sheds light on the idea that GSTO1 deletion show synthetic lethality with select DNA damaging drugs.

In this work, we employed CRISPR/Cas9 technologies coupling with extensive bioinformatics studies to validate GSTO1 as an impactful target in oncology. RNA transcription of all GSTO1 isoforms is downregulated and protein production is attenuated due to the CRISPR/CAS9 genome editing (Supplementary Fig. S12). To address the concern that CRISPR/Cas9 might produce off –target effect, we compared genetic results across multiple platforms with those of pharmacological inhibition of GSTO1. Mitomycin C, CB-839, and olaparib show differential activity in GSTO1 KO versus ntWT cells and are

also synergistic with C1–27. In addition to that, gene enrichment analysis in GSTO1 KO, siGSTO1-treated and C1–27- treated HCT116 cells reveals high consistency in transcriptional profiles including MYC and interferon pathways (Supplementary Fig. S13). We further compared the phenotypes of GSTO1 knockdown and GSTO1 KO in terms of cell growth (Supplementary Fig. S14) and proliferation upon glutamine starvation (Supplementary Fig. S15), which showed strong agreement between the two gene silencing methods. Thus, the phenotypes in GSTO1 KO cell lines are due to on target effect.

In conclusion, using an integrated genomics and proteomics platform we have uncovered GSTO1's involvement in multiple biological functions and pathways involved in cancer progression. We confirmed that GSTO1 expression is associated with reduced survival and tumor progression in multiple TCGA cohorts. Our study provides the first evidence that GSTO1 interferes with type I interferon response in cancer cells. We discovered *F3* transcription is down-regulated in response to GSTO1 KO and further implicating GSTO1 in tumor microenvironment. Clinical implication of this study is that PARP inhibitors, mitomycin-C and glutaminase inhibitor **CB-839** have significant synergy with the loss or inhibition of GSTO1. Together, these findings demonstrate the essential role of GSTO1 in tumor progression, shed light on its molecular signaling pathways, and further provide new insights on its potential use as a therapeutic target.

Supplementary Material

Refer to Web version on PubMed Central for supplementary material.

Acknowledgements

This work was supported by a grant from the NIH (CA193690). We thank Phillip L Palmbos and Yin Wang for their expertise on CRISPR/Cas9 genome editing. We thank Michelle Paulsen and Karan Bedi for conducting and helping with Bru-seq and data analysis. We thank Dr. Venkatesha Basrur (Mass Spectrometry-Based Proteomics Resource Facility, Department of Pathology, University of Michigan) for running the proteomics experiments. We thank Andrea Shergalis, Christine Cuthbertson, Ding Xue and Maha Zidan for reading early versions of this manuscript.

Reference

1. Yin ZL, Dahlstrom JE, Le Couteur DG, Board PG. Immunohistochemistry of omega class glutathione S-transferase in human tissues. J Histochem Cytochem 2001;49:983–7 [PubMed: 11457926]
2. Allocati N, Masulli M, Di Ilio C, Federici L. Glutathione transferases: substrates, inihibitors and pro-drugs in cancer and neurodegenerative diseases. Oncogenesis 2018;7:8 [PubMed: 29362397]
3. Board PG, Menon D. Structure, function and disease relevance of Omega-class glutathione transferases. Arch Toxicol 2016;90:1049–67 [PubMed: 26993125]
4. Li Y, Zhang Q, Peng B, Shao Q, Qian W, Zhang JY. Identification of glutathione S-transferase omega 1 (GSTO1) protein as a novel tumor-associated antigen and its autoantibody in human esophageal squamous cell carcinoma. Tumour Biol 2014;35:10871–7 [PubMed: 25085586]
5. Ramkumar K, Samanta S, Kyani A, Yang S, Tamura S, Ziemke E, et al. Mechanistic evaluation and transcriptional signature of a glutathione S-transferase omega 1 inhibitor. Nat Commun 2016;7:13084 [PubMed: 27703239]
6. Lombardi S, Fuoco I, di Fluri G, Costa F, Ricchiuti A, Biondi G, et al. Genomic instability and cellular stress in organ biopsies and peripheral blood lymphocytes from patients with colorectal cancer and predisposing pathologies. Oncotarget 2015;6:14852–64 [PubMed: 26046795]

7. Djukic T, Simic T, Pljesa-Ercegovac M, Matic M, Suvakov S, Coric V, et al. Upregulated glutathione transferase omega-1 correlates with progression of urinary bladder carcinoma. Redox Rep 2017;22:486–92 [PubMed: 28288548]
8. Piaggi S, Raggi C, Corti A, Pitzalis E, Mascherpa MC, Saviozzi M, et al. Glutathione transferase omega 1–1 (GSTO1–1) plays an anti-apoptotic role in cell resistance to cisplatin toxicity. Carcinogenesis 2010;31:804–11 [PubMed: 20106899]
9. Kodym R, Calkins P, Story M. The cloning and characterization of a new stress response protein. A mammalian member of a family of theta class glutathione s-transferase-like proteins. J Biol Chem 1999;274:5131–7 [PubMed: 9988762]
10. Tsuboi K, Bachovchin DA, Speers AE, Spicer TP, Fernandez-Vega V, Hodder P, et al. Potent and selective inhibitors of glutathione S-transferase omega 1 that impair cancer drug resistance. J Am Chem Soc 2011;133:16605–16 [PubMed: 21899313]
11. Lu H, Chen I, Shimoda LA, Park Y, Zhang C, Tran L, et al. Chemotherapy-induced Ca(2+) release stimulates breast cancer stem cell enrichment. Cell Rep 2017;18:1946–57 [PubMed: 28228260]
12. Kathryn Leake JS, Sharad S Singhal and Sanjay Awasthi. Apoptosis and differentiation of K562 cells by targeting GST-O1 to inhibit 4-HNE metabolism. Biochemistry & Pharmacology 2014;3
13. Li L, Zhao Y, Cao R, Li L, Cai G, Li J, et al. Activity-based protein profiling reveals GSTO1 as the covalent target of piperlongumine and a promising target for combination therapy for cancer. Chem Commun 2019;55:4407–10
14. Butturini E, Darra E, Chiavegato G, Cellini B, Cozzolino F, Monti M, et al. S-Glutathionylation at Cys328 and Cys542 impairs STAT3 phosphorylation. ACS Chem Biol 2014;9:1885–93 [PubMed: 24941337]
15. Carvalho AN, Marques C, Guedes RC, Castro-Caldas M, Rodrigues E, van Horssen J, et al. S-Glutathionylation of Keap1: a new role for glutathione S-transferase pi in neuronal protection. FEBS Lett 2016;590:1455–66 [PubMed: 27086966]
16. Menon D, Coll R, O'Neill LA, Board PG. Glutathione transferase omega 1 is required for the lipopolysaccharide-stimulated induction of NADPH oxidase 1 and the production of reactive oxygen species in macrophages. Free Radic Biol Med 2014;73:318–27 [PubMed: 24873723]
17. Hughes MM, McGettrick AF, O'Neill LAJ. Glutathione and glutathione transferase omega 1 as key posttranslational regulators in macrophages. Microbiol Spectr 2017;5
18. Menon D, Coll R, O'Neill LA, Board PG. GSTO1–1 modulates metabolism in macrophages activated through the LPS and TLR4 pathway. J Cell Sci 2015;128:1982–90 [PubMed: 25908843]
19. Hughes MM, Hooftman A, Angiari S, Tummala P, Zaslona Z, Runtsch MC, et al. Glutathione transferase omega-1 regulates NLRP3 inflammasome activation through NEK7 deglutathionylation. Cell Rep 2019;29:151–61 e5 [PubMed: 31577945]
20. Menon D, Innes A, Oakley AJ, Dahlstrom JE, Jensen LM, Brustle A, et al. GSTO1–1 plays a pro-inflammatory role in models of inflammation, colitis and obesity. Sci Rep 2017;7:17832 [PubMed: 29259211]
21. Broad Institute TCGA Genome Data Analysis Center. Firehose stddata__2016_01_28 run 2016.
22. R Core Team. R: A language and environment for statistical computing. R Foundation for Statistical Computing: Vienna, Austria,; 2019.
23. Subramanian A, Tamayo P, Mootha VK, Mukherjee S, Ebert BL, Gillette MA, et al. Gene set enrichment analysis: A knowledge-based approach for interpreting genome-wide expression profiles. Proc Natl Acad Sci U S A 2005;102:15545–50 [PubMed: 16199517]
24. Paulsen MT, Veloso A, Prasad J, Bedi K, Ljungman EA, Magnuson B, et al. Use of Bru-Seq and BruChase-Seq for genome-wide assessment of the synthesis and stability of RNA. Methods 2014;67:45–54 [PubMed: 23973811]
25. Harrow J, Frankish A, Gonzalez JM, Tapanari E, Diekhans M, Kokocinski F, et al. GENCODE: The reference human genome annotation for The ENCODE Project. Genome Res 2012;22:1760–74 [PubMed: 22955987]
26. Dobin A, Davis CA, Schlesinger F, Drenkow J, Zaleski C, Jha S, et al. STAR: ultrafast universal RNA-seq aligner. Bioinformatics 2013;29:15–21 [PubMed: 23104886]

27. Trapnell C, Williams BA, Pertea G, Mortazavi A, Kwan G, van Baren MJ, et al. Transcript assembly and quantification by RNA-Seq reveals unannotated transcripts and isoform switching during cell differentiation. Nat Biotechnol 2010;28:511–U174 [PubMed: 20436464]
28. Liao Y, Smyth GK, Shi W. featureCounts: an efficient general purpose program for assigning sequence reads to genomic features. Bioinformatics 2014;30:923–30 [PubMed: 24227677]
29. Love MI, Huber W, Anders S. Moderated estimation of fold change and dispersion for RNA-seq data with DESeq2. Genome Biol 2014;15
30. Edgar R, Domrachev M, Lash AE. Gene Expression Omnibus: NCBI gene expression and hybridization array data repository. Nucleic Acids Res 2002;30:207–10 [PubMed: 11752295]
31. Fresno C, Fernandez EA. RDAVIDWebService: a versatile R interface to DAVID. Bioinformatics 2013;29:2810–1 [PubMed: 23958726]
32. Zhu AQ, Ibrahim JG, Love MI. Heavy-tailed prior distributions for sequence count data: removing the noise and preserving large differences. Bioinformatics 2019;35:2084–92 [PubMed: 30395178]
33. Baker BM, Chen CS. Deconstructing the third dimension - how 3D culture microenvironments alter cellular cues. J Cell Sci 2012;125:3015–24 [PubMed: 22797912]
34. Ricci-Vitiani L, Pallini R, Biffoni M, Todaro M, Invernici G, Cenci T, et al. Tumour vascularization via endothelial differentiation of glioblastoma stem-like cells. Nature 2010;468:824–U121 [PubMed: 21102434]
35. Li YJ, Scott WK, Zhang L, Lin PI, Oliveira SA, Skelly T, et al. Revealing the role of glutathione S-transferase omega in age-at-onset of Alzheimer and Parkinson diseases. Neurobiol Aging 2006;27:1087–93 [PubMed: 15985314]
36. Kim Y, Cha SJ, Choi HJ, Kim K. Omega class glutathione S-transferase: antioxidant enzyme in pathogenesis of neurodegenerative diseases. Oxid Med Cell Longev 2017;2017:5049532 [PubMed: 29435097]
37. Peretz L, Besser E, Hajbi R, Casden N, Ziv D, Kronenberg N, et al. Combined shRNA over CRISPR/cas9 as a methodology to detect off-target effects and a potential compensatory mechanism. Sci Rep 2018;8
38. Vogel C, Marcotte EM. Insights into the regulation of protein abundance from proteomic and transcriptomic analyses. Nat Rev Genet 2012;13:227–32 [PubMed: 22411467]
39. Szablewski L Expression of glucose transporters in cancers. Biochim Biophys Acta 2013;1835:164–9 [PubMed: 23266512]
40. Osthus RC, Shim H, Kim S, Li Q, Reddy R, Mukherjee M, et al. Accelerated publication - Deregulation of glucose transporter 1 and glycolytic gene expression by c-Myc. J Biol Chem 2000;275:21797–800 [PubMed: 10823814]
41. Schwartzenberg-Bar-Yoseph F, Armoni M, Karnieli E. The tumor suppressor p53 down-regulates glucose transporters GLUT1 and GLUT4 gene expression. Cancer Res 2004;64:2627–33 [PubMed: 15059920]
42. Critchley-Thorne RJ, Simons DL, Yan N, Miyahira AK, Dirbas FM, Johnson DL, et al. Impaired interferon signaling is a common immune defect in human cancer. Proc Natl Acad Sci U S A 2009;106:9010–5 [PubMed: 19451644]
43. Zhang JF, Chen Y, Lin GS, Zhang JD, Tang WL, Huang JH, et al. High IFIT1 expression predicts improved clinical outcome, and IFIT1 along with MGMT more accurately predicts prognosis in newly diagnosed glioblastoma. Hum Pathol 2016;52:136–44 [PubMed: 26980050]
44. Hisada Y, Mackman N. Tissue factor and cancer: regulation, tumor growth, and metastasis. Semin Thromb Hemost 2019;45:385–95 [PubMed: 31096306]
45. Hu ZW, Xu J, Cheng JJ, McMichael E, Yu LB, Carson WE. Targeting tissue factor as a novel therapeutic oncotarget for eradication of cancer stem cells isolated from tumor cell lines, tumor xenografts and patients of breast, lung and ovarian cancer. Oncotarget 2017;8:1481–94 [PubMed: 27903969]
46. Yan XD, Pan LY, Yuan Y, Lang JH, Mao N. Identification of platinum-resistance associated proteins through proteomic analysis of human ovarian cancer cells and their platinum-resistant sublines. J Proteome Res 2007;6:772–80 [PubMed: 17269733]

47. Manupati K, Debnath S, Goswami K, Bhoj PS, Chandak HS, Bahekar SP, et al. Glutathione S-transferase omega 1 inhibition activates JNK-mediated apoptotic response in breast cancer stem cells. FEBS J 2019;286:2167–92 [PubMed: 30873742]
48. Martinez FO, Helming L, Milde R, Varin A, Melgert BN, Draijer C, et al. Genetic programs expressed in resting and IL-4 alternatively activated mouse and human macrophages: similarities and differences. Blood 2013;121:E57–E69 [PubMed: 23293084]
49. Parker BS, Rautela J, Hertzog PJ. Antitumour actions of interferons: implications for cancer therapy. Nat Rev Cancer 2016;16:131–44 [PubMed: 26911188]
50. Di Franco S, Turdo A, Todaro M, Stassi G. Role of type I and II interferons in colorectal cancer and melanoma. Front Immunol 2017;8:878 [PubMed: 28798748]
51. Stine ZE, Walton ZE, Altman BJ, Hsieh AL, Dang CV. MYC, metabolism, and cancer. Cancer Discov 2015;5:1024–39 [PubMed: 26382145]
52. Kent LN, Leone G. The broken cycle: E2F dysfunction in cancer. Nat Rev Cancer 2019;19:326–38 [PubMed: 31053804]
53. Menon D, Board PG. A role for glutathione transferase Omega 1 (GSTO1–1) in the glutathionylation cycle. J Biol Chem 2013;288:25769–79 [PubMed: 23888047]
54. Versteeg HH. Tissue factor: old and new links with cancer biology. Semin Thromb Hemost 2015;41:747–55 [PubMed: 26408927]
55. Rong Y, Hu F, Huang R, Mackman N, Horowitz JM, Jensen RL, et al. Early growth response gene-1 regulates hypoxia-induced expression of tissue factor in glioblastoma multiforme through hypoxia-inducible factor-1-independent mechanisms. Cancer Res 2006;66:7067–74 [PubMed: 16849552]
56. Krikun G, Schatz F, Mackman N, Guller S, Demopoulos R, Lockwood CJ. Regulation of tissue factor gene expression in human endometrium by transcription factors Sp1 and Sp3. Mol Endocrinol 2000;14:393–400 [PubMed: 10707957]
57. Yeh HH, Chang WT, Lu KC, Lai WW, Liu HS, Su WC. Upregulation of tissue factor by activated Stat3 contributes to malignant pleural effusion generation via enhancing tumor metastasis and vascular permeability in lung adenocarcinoma. PLoS One 2013;8:e75287 [PubMed: 24086497]
58. Parry GCN, Mackman N. Transcriptional regulation of tissue factor expression in human endothelial-cells. Arterioscl Throm Vas 1995;15:612–21
59. Coll RC, Robertson A, Butler M, Cooper M, O'Neill LA. The cytokine release inhibitory drug CRID3 targets ASC oligomerisation in the NLRP3 and AIM2 inflammasomes. PLoS One 2011;6:e29539 [PubMed: 22216309]
60. Terry CM, Callahan KS. Protein kinase C regulates cytokine-induced tissue factor transcription and procoagulant activity in human endothelial cells. J Lab Clin Med 1996;127:81–93 [PubMed: 8592100]
61. Yu JL, May L, Lhotak V, Shahrzad S, Shirasawa S, Weitz JI, et al. Oncogenic events regulate tissue factor expression in colorectal cancer cells: implications for tumor progression and angiogenesis. Blood 2005;105:1734–41 [PubMed: 15494427]
62. Ricks TK, Chiu HJ, Ison G, Kim G, McKee AE, Kluetz P, et al. Successes and challenges of PARP inhibitors in cancer therapy. Front Oncol 2015;5:222 [PubMed: 26528434]
63. Srinivas US, Tan BWQ, Vellayappan BA, Jeyasekharan AD. ROS and the DNA damage response in cancer. Redox Biol 2018:101084 [PubMed: 30612957]
64. Hou D, Liu ZJ, Xu XH, Liu Q, Zhang XY, Kong BH, et al. Increased oxidative stress mediates the antitumor effect of PARP inhibition in ovarian cancer. Redox Biol 2018;17:99–111 [PubMed: 29684820]
65. Lee SY, Lim IA, Kang GU, Cha SJ, Altanbyek V, Kim HJ, et al. Protective effect of Drosophila glutathione transferase omega 1 against hydrogen peroxide-induced neuronal toxicity. Gene 2015;568:203–10 [PubMed: 26024591]

Significance

Findings validate GSTO1 as a therapeutic target in cancer and implicate GSTO1 in the modulation of tumor growth, immune responses, and expression of F3.

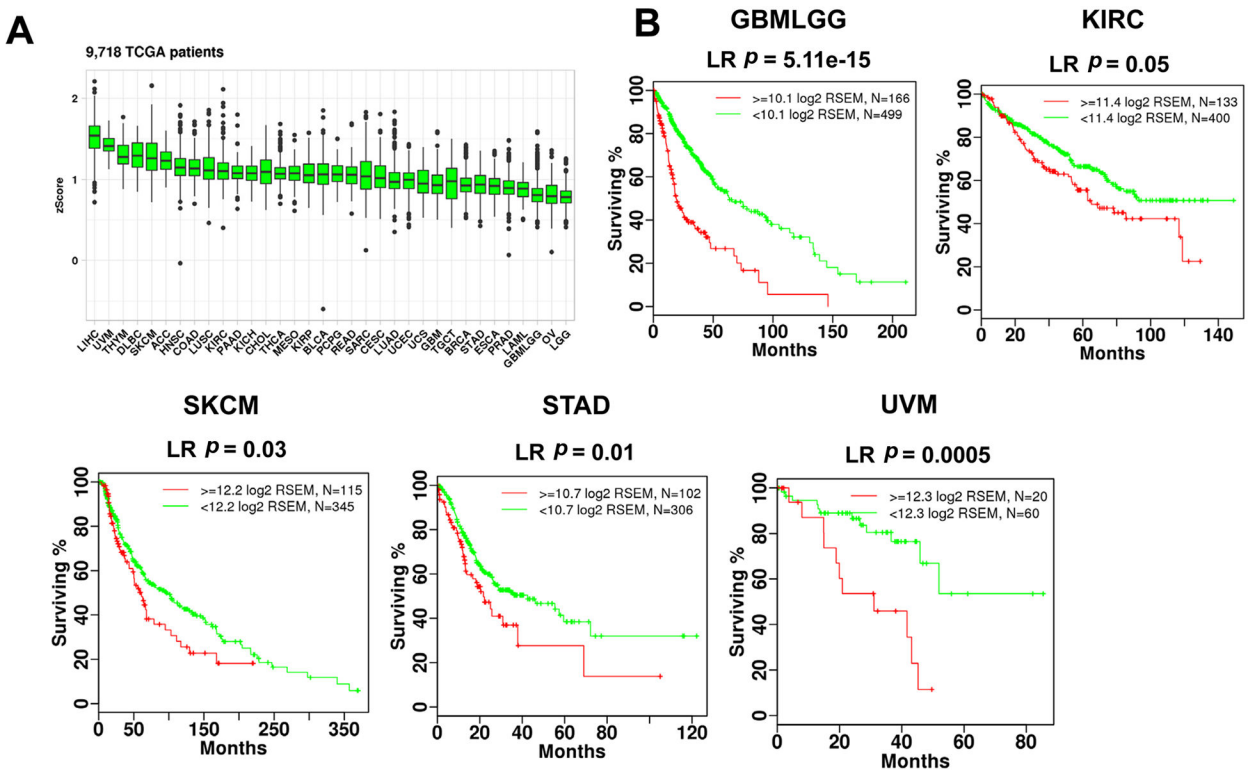

Figure 1.

GSTO1 is up-regulated in select cancers and correlates with decreased patient survival. **A**, above average expression of GSTO1 was detected across 34 TCGA diseases. **B**, Kaplan-Meier analysis of five cancer types identified as lower patient survival correlated to higher expression of GSTO1. Patients stratified using 75% expression percentile.

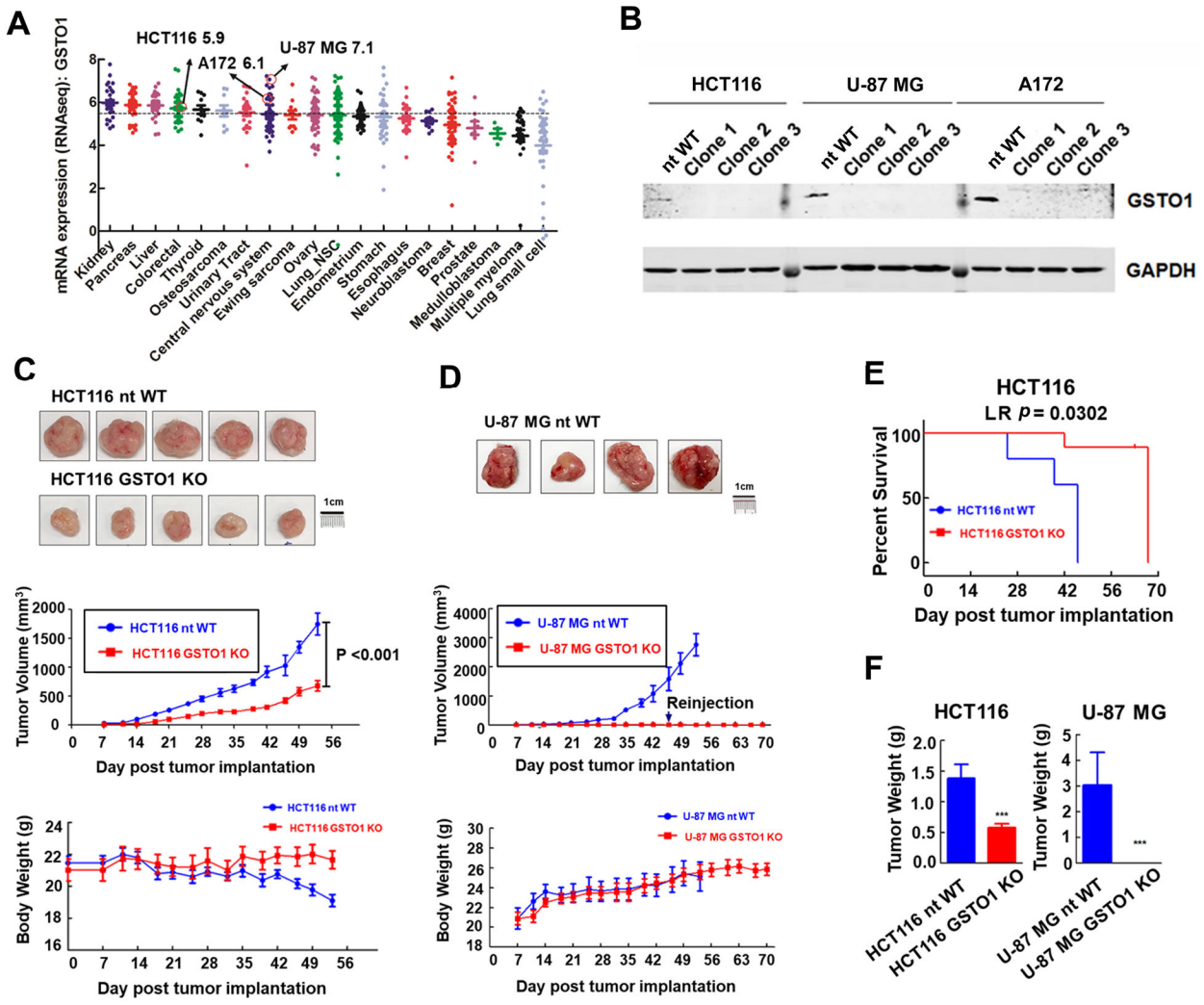

Figure 2.

Knockout of GSTO1 impairs tumor growth *in vivo*. **A**, GSTO1 mRNA expression in CCLE cell lines among 20 types of cancers. Dashed line shows the average expression of GSTO1 across all cell types. HCT116, U-87 MG and A172 all showed above average GSTO1 expression.

B, GSTO1 protein expression in single clones of cell lines HCT116, U-87 MG, and A172 transfected with non-targeting (nt WT) or GSTO1 targeting crRNA/tracrRNA (GSTO1 KO). **C**, tumor growth of HCT116 nt WT and GSTO1 KO cells implanted subcutaneously in ICRSC mice. Statistical difference was determined by two-way ANOVA. Changes in body weight of mice are shown on the lower panel. **D**, tumor growth of U-87 MG nt WT and GSTO1 KO cells implanted subcutaneously in ICRSC mice. nt WT tumor group was terminated when the tumors reached 2000 mm3. GSTO1 KO group was terminated 10 weeks after tumor implantation. Changes in body weight of mice are shown on the lower panel.. **E**, Kaplan-Meier curve of an independent xenograft study with HCT116 nt WT and GSTO1 KO cells implanted subcutaneously in NOD/SCID mice. **F**, Tumor weights of mice

with nt WT and GSTO1 KO cell implantation after necropsy. Statistical difference was determined by Student's *t*-test (*** $p<0.001$).

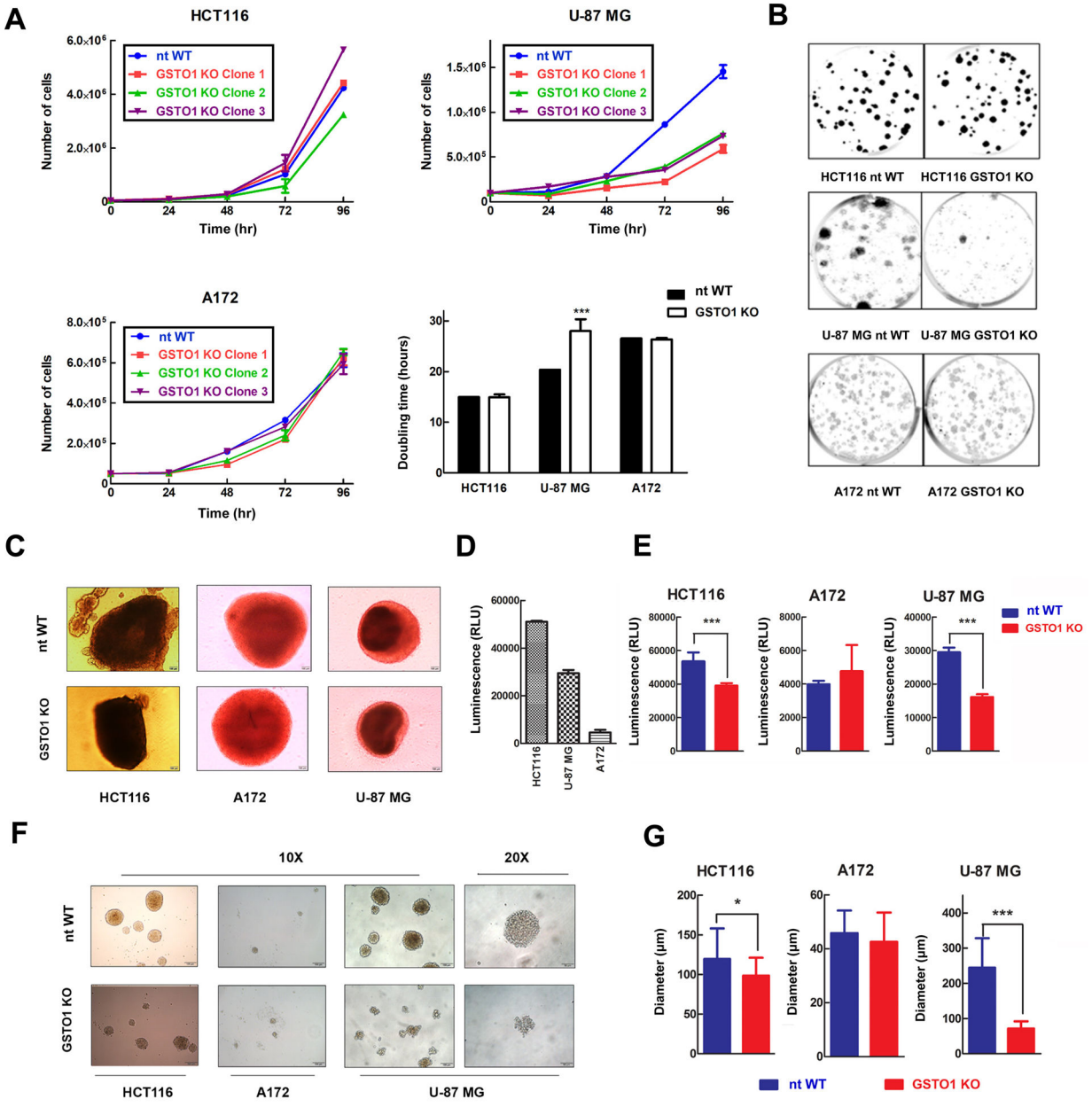

Figure 3.

Deletion of GSTO1 reduces U-87 MG cell proliferation, impedes the growth of 3D tumor spheroids and neuro-sphere formation of U-87 MG and HCT116 cells. **A**, Doubling time of HCT116, U-87 MG and A172 nt WT and GSTO1 KO single clones. Same number of nt WT and GSTO1 KO cells were seeded. After 24, 48, 72 and 96 hours, cells were harvested and counted manually. **B**, Representative images of colony–forming abilities of HCT116, U-87 MG and A172 nt WT and GSTO1 KO cell lines. Representative images of HCT116, A172 and U-87 MG nt WT and GSTO1 KO tumor spheroid growth (**C**). CellTiter-Glo® 3D cell viability assay was used for quantification seven days after seeding (**D-E**). Representative images of HCT116, A172 and U-87 MG nt WT and GSTO1 KO spheroids (**F**). Spheroids were grown in ultra-low attachment wells in medium without FBS. Diameters were

calculated with at least 20 spheroids using ImageJ (**G**). Statistical difference was determined by Student's *t*-test (*** $p<0.001$).

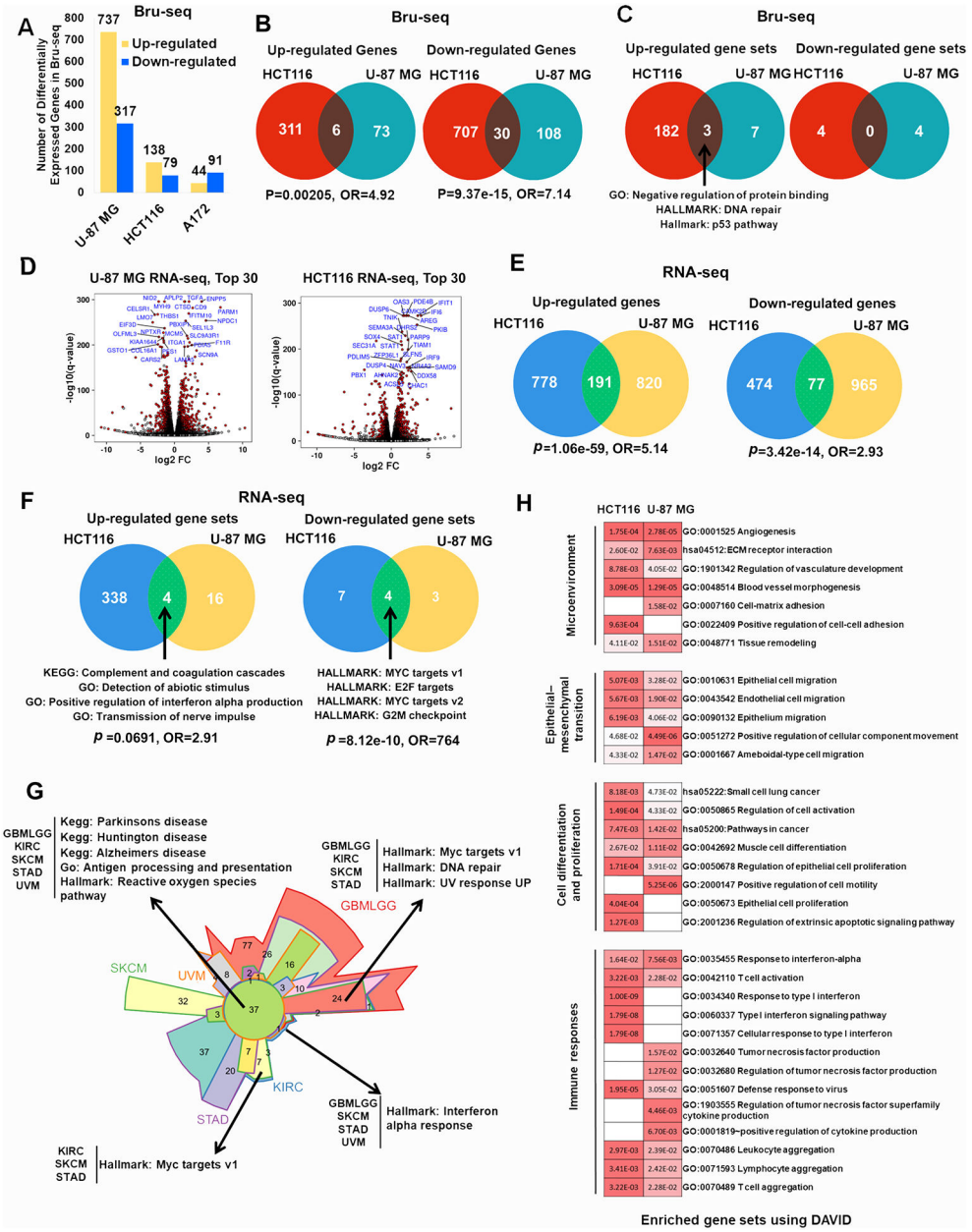

Figure 4.

Integrated transcriptional profiles across cell lines reveals that GSTO1 dysregulates critical pathways in cancer. **A**, Number of differentially expressed genes upon GSTO1 KO in Bru-seq transcription profile in U-87 MG, HCT116 and A172 cells. **B**, Significantly changed genes overlapped in nascent (Bru-seq) transcriptomic profiles of HCT116, U-87 MG and A172 cells in response to GSTO1 KO. **C**, Common significantly changed gene sets (GSEA) overlapped in nascent (Bru-seq) transcriptomic profiles between HCT116 and U-87 MG cells in response to GSTO1 KO. **D**, Volcano plots of RNA-seq genes differentially expressed upon GSTO1 KO in U-87 MG and HCT116 cells. Top 30 differentially expressed genes are highlighted. **E**, Significantly changed genes overlapped in RNA-seq between HCT116 and U-87 MG cells in response to GSTO1 KO. **F**, Common significantly changed gene sets

(GSEA) overlapped in transcriptomic profiles (RNA-seq) between HCT116 and U-87 MG cells in response to GSTO1 KO. **G**, Gene sets commonly enriched with up-regulated GSTO1 expression across GBMLGG, KIRC, STAD, UVM and SKCM. Shared gene sets are highlighted along with the disease type. Differential expression thresholds are described in the Materials and Methods section. Gene sets with FDR<0.1 were considered as significant. **H**, Gene sets enriched for up- and down- regulated genes using DAVID in HCT116 and U-87 MG RNA-seq. The enrichment of gene sets involved in the tumor microenvironment, epithelial-to-mesenchymal transition, proliferation and differentiation and immune responses are highlighted.

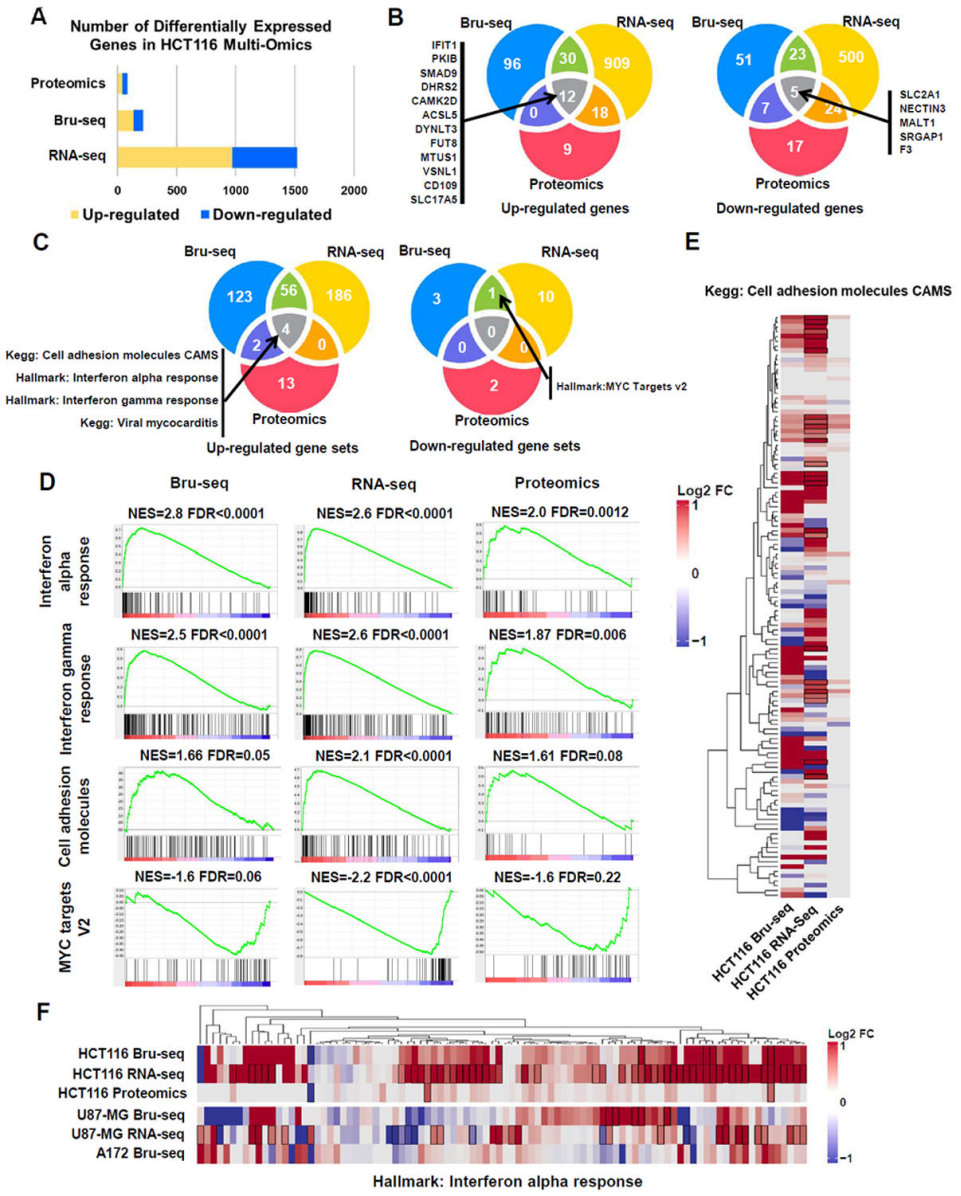

Figure 5.

Multi-omics analysis of HCT116 in response to GSTO1 deletion leads to the enrichment of cell adhesion, interferon alpha and interferon gamma response gene sets. **A**, Number of differentially expressed genes as a result of GSTO1 KO across the three platforms. Differential expression thresholds used per platform are described in the Methods section. **B**, Sixteen genes were commonly up- (four) or down- (twelve) regulated across all three profiling platforms. **C**, Significantly changed gene sets (GSEA) overlapped among the three omics platforms. Up-regulated gene sets include cell adhesion molecules, interferon alpha response, interferon gamma response and viral myocarditis. Gene sets with FDR<0.1 were considered significant. **D**, GSEA plots for gene sets enriched in multi-omics. NES = normalized enrichment score; FDR= false discovery rate. **E-F**, Heatmap showing log2 fold

changes of 107 expressed genes belonging to the cell adhesion molecules gene set and interferon alpha response gene set. Differentially expressed genes have black border.

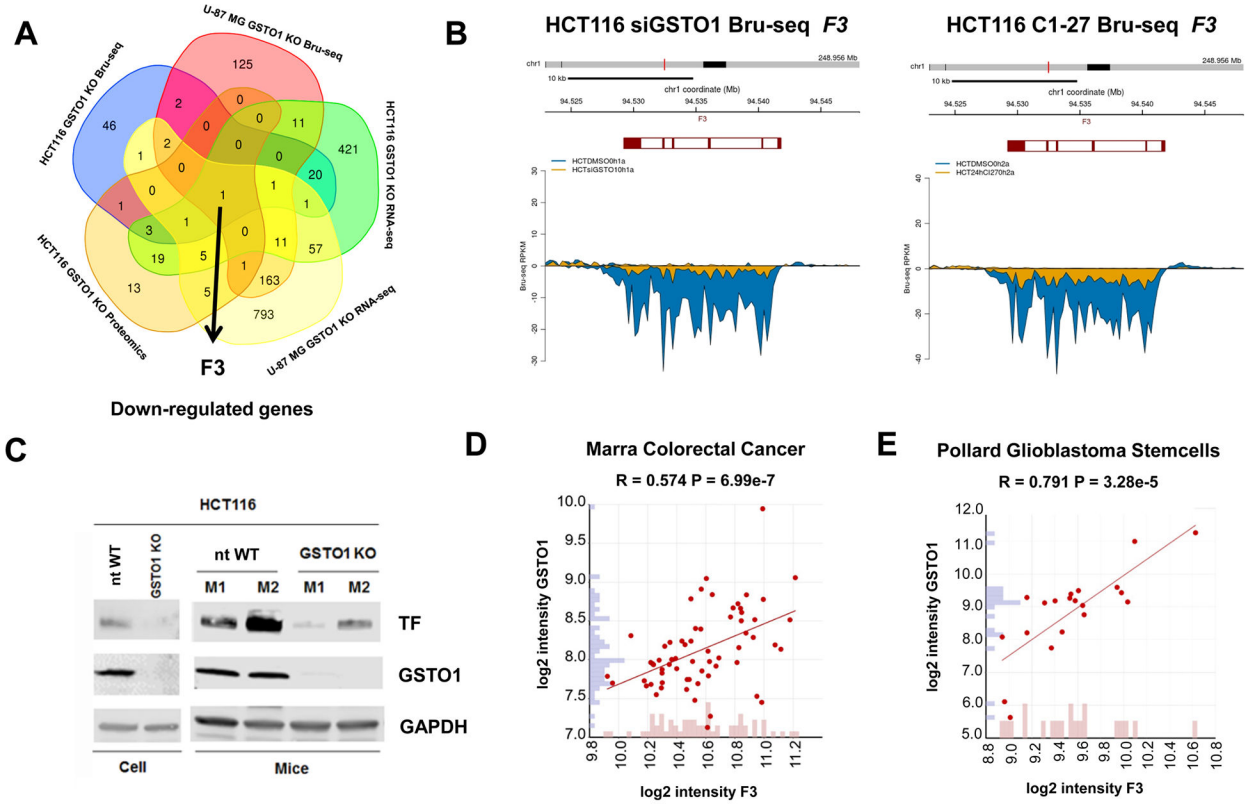

Figure 6.

Deletion of GSTO1 suppresses F3 transcription and TF expression. **A**, Venn diagram illustrating commonly down-regulated genes among Bru-seq, RNA-seq and proteomic in HCT116 and Bru-seq, RNA-seq in U-87 MG . F3 is shared by five platforms and cell lines. **B**, Bru-Seq gene trace of F3 after GSTO1 inhibitor C1–27 treatment or siGSTO1 treatment in HCT116 cells. Correlation between F3 and GSTO1 in colorectal cancer (Marra colorectal cancer database) (**C**) and glioblastoma stem cells (Pollard glioblastoma stemcells database) (**D**) from the R2: Genomics Analysis and Visualization Platform (http://r2.amc.nl).

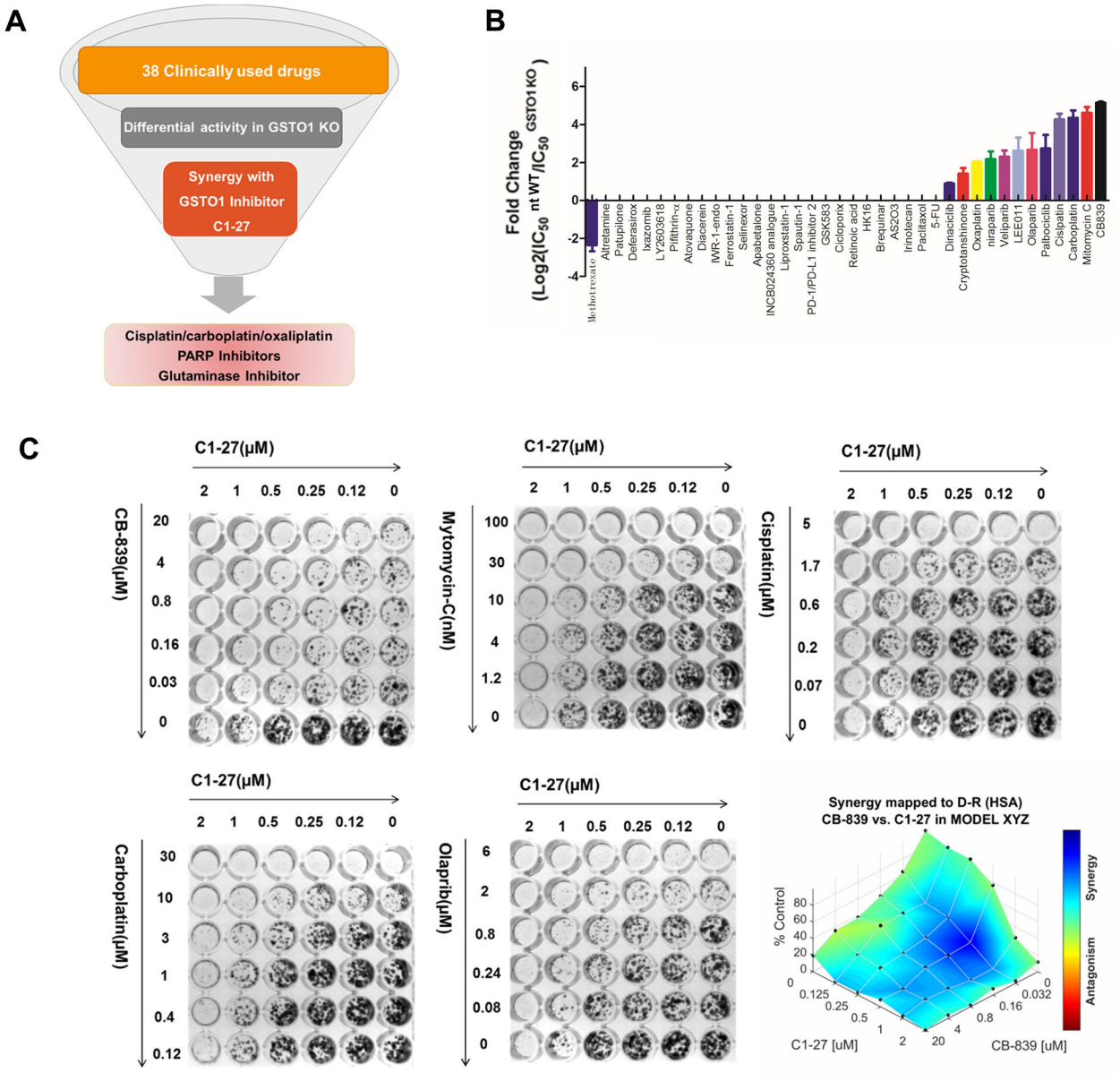

Figure 7.

PARP inhibitors and glutaminase inhibitor **CB-839** are synthetically lethal with the loss of GSTO1. **A**, Workflow for the lead identification in the HCT116 GSTO1 KO cell line. **B**, Thirty-eight clinical and preclinical drugs were tested on HCT116 nt WT and GSTO1 KO cell lines. IC_{50} values in each cell line were calculated by the intensity of crystal violet staining in colony formation assay wells (ImageJ). Differential index is illustrated by $\log_2$ (IC_{50} of HCT116 nt WT / IC_{50} of GSTO1 KO) and determined by three independent experiments. **C**, HCT116 cells were treated with indicated concentrations of CB-839, cisplatin, carboplatin, or olaparib, in combination with **C1–27** for 7 days, and stained with crystal violet. The intensity of each well was calculated using ImageJ. The synergistic effect of **C1–27** with **CB-839** is illustrated with HSA model.